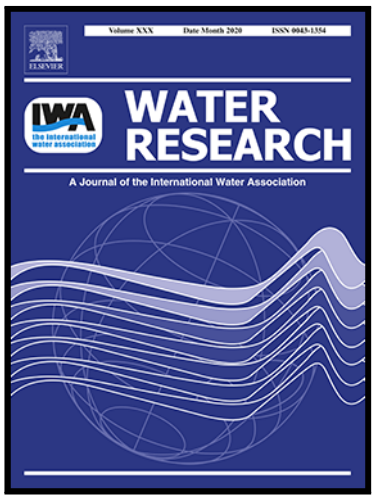

Rapid Oxidation of Histamine H_2-Receptor Antagonists by Peroxymonosulfate during Water Treatment: Kinetics, Products, and Toxicity Evaluation

Yajie Qian , Jinjing Huang , Xiang Liu , Tongcai Liu , Gang Xue , Pin Gao , Xuefei Zhou , Yalei Zhang , Jiabin Chen

PII: S0043-1354(20)30815-0
DOI: https://doi.org/10.1016/j.watres.2020.116278
Reference: WR 116278

To appear in: *Water Research*

Received date: 24 April 2020
Revised date: 29 July 2020
Accepted date: 6 August 2020

Please cite this article as: Yajie Qian , Jinjing Huang , Xiang Liu , Tongcai Liu , Gang Xue , Pin Gao , Xuefei Zhou , Yalei Zhang , Jiabin Chen , Rapid Oxidation of Histamine H_2-Receptor Antagonists by Peroxymonosulfate during Water Treatment: Kinetics, Products, and Toxicity Evaluation, *Water Research* (2020), doi: https://doi.org/10.1016/j.watres.2020.116278

Highlights

- PMS exhibits specific and high reactivity towards HRAs
- HRAs oxidation by PMS proceeds via a non-radical process
- PMS-promoted HRAs degradation is unaffected by water matrices
- Thioether sulfur in HRAs (except RXTD) is oxidized to sulfoxide product
- Ecotoxicity of HRAs is remarkably reduced after PMS oxidation

Rapid Oxidation of Histamine H_2-Receptor Antagonists by Peroxymonosulfate during Water Treatment: Kinetics, Products, and Toxicity Evaluation

Yajie Qian[a], Jinjing Huang[a], Xiang Liu[a], Tongcai Liu[b], Gang Xue[a], Pin Gao[a], Xuefei Zhou[b], Yalei Zhang[b,c], Jiabin Chen[b,c,*]

[a] *College of Environmental Science and Engineering, Donghua University, Shanghai, 201620, P. R. China*

[b] *State Key Laboratory of Pollution Control and Resources Reuse, College of Environmental Science and Engineering, Tongji University, Shanghai 200092, China*

[c] *Shanghai Institute of Pollution Control and Ecological Security, Shanghai, 200092, P.R. China*

* Corresponding Author.

Phone: 86-21-65985811; Fax: 86-21-65986960.

Email: chenjiabincn@163.com (Jiabin Chen).

Manuscript submitted to

Water Research

Abstract

Peroxymonosulfate (PMS) is an appealing oxidant for organic contaminant destruction relying on radical generation after activation. Herein, we report PMS-promoted rapid degradation of histamine H_2-receptor antagonists (HRAs) through non-radical process for the first time. Five commonly used HRAs, i.e., ranitidine (RNTD), cimetidine (CMTD), famotidine (FMTD), nizatidine (NZTD) and roxatidine (RXTD), were examined their reactivity towards PMS. Results show that HRAs (except RXTD) exhibit high reactivity towards PMS, with apparent second-order rate constants from 403 to 872 $M^{-1}s^{-1}$ at pH 7.0. Radical scavenging experiments excluded the contribution of radicals to PMS-promoted degradation of HRAs, and this non-radical process was unaffected by the real water matrices. Structure-activity assessment and theoretical calculation indicated that the thioether sulfur in HRAs (except RXTD) was the main reactive site for PMS oxidation. Transformation product analysis further elucidated oxidation of the thioether sulfur to sulfoxide product through an oxygen atom transfer process. Moreover, the thioether sulfur on the straight chain was more susceptible to oxygen transfer with PMS than that on the thiazole ring of HRAs. Toxicity evaluation indicated the ecotoxicity of HRAs could be remarkably reduced after PMS oxidation. Hence, this work provides a promising strategy to rapidly remove HRAs and significantly reduce their toxicity in water treatment.

Keywords: Histamine H_2-receptor antagonists; Peroxymonosulfate; Non-radical process; Thioether sulfur.

1. Introduction

Histamine H_2-receptor antagonists (HRAs) are gastrointestinal drugs extensively used to inhibit gastric acid secretion through blockade of histamine H_2-receptors in the gastric mucosa (Ganellin et al. 1976, Ikehata et al. 2006a). The commonly used HRAs include ranitidine (RNTD), cimetidine (CMTD), famotidine (FMTD), nizatidine (NZTD) and roxatidine (RXTD) (Figure 1). After administration, a substantial portion of HRAs are excreted unchanged, and finally discharged into the environment, and thus they have been widely detected in the wastewater, surface water and even sediments (Andreozzi et al. 2003, Buth et al. 2007, Choi et al. 2008, Kolpin et al. 2002, Radjenović et al. 2009, Zuccato et al. 2000). For example, FMTD, RNTD and CMTD were detected in the wastewater effluent up to 5.38 μg/L (Choi et al. 2008, Radjenović et al. 2009). RNTD and CMTD were found to occur in the surface water at concentrations ranging from 10 to 580 ng/L (Kolpin et al. 2002, Zuccato et al. 2000), and RNTD has been regarded as one of the highest risk pharmaceuticals in the surface water (Besse and Garric 2008). The occurrence of HRAs in the environment may exert biological effects on non-target organisms, and thus raises potential risk to the ecosystem and public health.

Generally, biological treatment processes were reported to be ineffective to remove HRAs in wastewater treatment plants (Radjenović et al. 2009); while oxidative water treatment is an important method to degrade HRAs. Disinfection unit is a significant sink for HRAs before HRAs discharging to the environment. HRAs, e.g., CMTD, are susceptible to

rapid oxidation by free chlorine and chloramines, generating some unexpected products with higher toxicity (Buth et al. 2007). Ozonation was found to be effective in oxidizing nitro-HRAs, e.g., RNTD and NZTD, but the oxidized products had higher potential to form halonitromethanes (TCNM), which show high cytotoxicity and genotoxicity and thus have been regulated (Wang et al. 2016). Although nitro-HRAs are photo-reactive under UV irradiation, UV intensity currently used in disinfection could not fully eliminate HRAs and their TCNM formation potential (Dong et al. 2017). Hence, more efficient and clean techniques are required to remove these HRAs from wastewater effectively.

Persulfate (PS), including peroxymonosulfate (PMS) and peroxydisulfate (PDS), have become emerging oxidants in wastewater treatment (Zhang et al. 2015a). The homogeneous cleavage of peroxide bond in PS can generate reactive radical species, e.g., $SO_4^{\bullet-}$ (Chen et al. 2019b). Activation of PS to generate $SO_4^{\bullet-}$ is generally considered to be crucial for contaminant destruction in wastewater treatment (Qian et al. 2018). Various strategies have been used to activate PS for $SO_4^{\bullet-}$ generation, including electron transfer reaction (e.g., activation with transition metal (Anipsitakis and Dionysiou 2004) or base (Furman et al. 2010)) and external energy stimulation (e.g., UV (Zhang et al. 2015b, Zhou et al. 2018a) and heating (Chen et al. 2016a, Gao et al. 2016)). $SO_4^{\bullet-}$ is a strong oxidant with high redox potential (E^0 = 2.5-3.1 V), and thus can degrade a broad range of contaminants (Chen et al. 2016b). However, $SO_4^{\bullet-}$ is non-selective, and thus also shows high reactivity towards water matrices, e.g. , Cl^-, HCO_3^-, and natural organic matters (Qian et al. 2016), which might reduce the treatment efficiency in the real water matrices. Recently, the non-radical process with PS has received considerable concerns owing to its high selectivity towards target contaminants

(Duan et al. 2018). PMS was reported to effectively oxidize some organic contaminants without activation, and such reaction is significantly dependent on the contaminant structure (Yang et al. 2018). For example, PMS shows specific and high reactivity towards β-lactam antibiotics (Chen et al. 2018), fluoroquinolone (Zhou et al. 2018b), sulfonamides (Ji et al. 2018, Yin et al. 2018), and thioether sulfur, N_4 amine on piperazine ring, and amino group on the benzene were regarded as the effective sites for PMS oxidation, respectively. HRAs seem to be reactive towards various oxidants due to the presence of multiple reactive moieties/groups, such as furan ring, amine and thioether sulfur (Ikehata et al. 2006b). However, it is still unclear whether PMS can degrade HRAs.

In this work, we found PMS exhibited specific and high reactivity towards some HRAs without external energy or activators. This new discovery motivated us to conduct an in-depth study to address two major research questions: (1) How PMS reacts with HRAs, and (2) What characteristics render HRAs highly reactive towards PMS. To our best knowledge, this study is among the first to systematically reveal the specific and rapid reaction between PMS and HRAs. The new findings of this study provide a promising and facile strategy to eliminate HRAs contamination in wastewater treatment.

2. Materials and methods

2.1 Chemicals

The standard chemicals of FMTD, RNTD, CMTD, NZTD and RXTD were purchased from Sigma-Aldrich or ANPEL laboratory Technologies (Shanghai) Inc. at the highest purity. PMS

and PDS were obtained from Sigma-Aldrich at > 99% purity. Methanol (MeOH), acetonitrile and *tert*-butyl alcohol (TBA), formic acid, and ammonium acetate were also obtained from Sigma-Aldrich at HPLC grade. Hydrogen peroxide (HP, H_2O_2), sodium thiosulfate ($Na_2S_2O_3$), sodium dihydrogen phosphate (NaH_2PO_4), disodium hydrogen phosphate (Na_2HPO_4), sodium chloride (NaCl), sodium bicarbonate ($NaHCO_3$), sodium hydroxide (NaOH), humic acid, and sulfuric acid (H_2SO_4) were obtained from Sinopharm Chemical Reagent Co., Ltd at analytical grade. Deionized (DI) reagent water was produced from a Millipore Milli-Q Ultrapure Gradient A10 purification system.

2.2 Real water samples

Surface water (SW) from a river and municipal wastewater (MWW) were collected at locations in the southeast region of China. Samples were filtered through 0.45-μm glass fiber filters immediately upon collection and stored at 5 °C before use. The characteristics of the samples are shown in Tables S1. A synthetic hospital wastewater (HWW) was prepared by adopting recipes (Serna-Galvis et al. 2017), and also used to evaluate the efficiency of HRAs degradation. The composition of HWW is shown in Table S2.

2.3 Experimental procedures

Experiments were conducted in amber glass serum bottles at room temperature (22 °C). Reaction pH was maintained with 10 mM phosphate buffer. Reaction solutions were prepared with HRAs and buffer, and then PMS was added to initiate the reaction. Samples were collected at the predetermined time and quenched with 100 μL of 1 M sodium thiosulfate ($Na_2S_2O_3$), which could completely consume the remaining PMS. The initial concentrations

used for HRAs and PMS were 10 and 100 μM, respectively, for most experiments. 10-500 μM of PMS were added to the HRAs solution to evaluate the impact of PMS concentration. Radical quenchers (i.e., MeOH and TBA) were added to investigate whether the radicals contributed to the degradation of HRAs. Cl^-, HCO_3^-, and humic acid were spiked into the reaction solution to evaluate the impact of water matrices. The above reactions were also conducted in the real water matrices, i.e., SW, MWW, and HWW. All the experiments were conducted in duplicate or more.

2.4 Analytical methods

HRAs were analyzed by a high performance liquid chromatograph (HPLC, 1260, Agilent Technology, USA) equipped with a UV detector. Samples with 15 μL injection was separated on a Kromasil-C18 column (4.6 × 250 mm, 5 μm). The details are provided in Table S3.

Transformation products were determined on a HPLC system (Utimate 3000, Dionex, USA) connected to a triple quadrupole mass spectrometer (TSQ Quantum Ultra EMR, Thermo Fisher Scientific, USA) with electrospray ionization (ESI). Samples with 40 μL injection were separated on a Zorbax SB-C18 column (2.1 × 150 mm, 5 μm). The detailed conditions are summarized in Text S1.

PMS was analyzed by a spectrophotometric method proposed by Liang et al. (Liang et al. 2008), as detailed in Text S2.

2.5 Theoretical calculation

The frontier electron density (FED) calculations were conducted by the Gaussian 09 program on a basis set of B3LYP/6-31 G (d, p). The FEDs of the highest occupied molecular orbital (HOMO) were obtained and visualized. Condensed Fukui function based on the density functional theory (DFT) was used to predict the regioselectivity of different reactive species on the HRAs molecules.

2.6 Ecotoxicity assessment

The ecotoxicity of HRAs and the oxidized products were evaluated using the Ecological Structure-Activity Relationship Model (ECOSAR) program (Liu et al. 2018). This program has been successfully used to predict the ecotoxicity to screen contaminants. The ecotoxicity was assessed for three trophic levels of aquatic organisms, i.e., fish, daphnid and green algae. Half Lethal Concentration (LC_{50}) values for fish (96 h), daphnid (48 h), and Half Effective Concentration (EC_{50}) values for algae (96 h) were used to assess the acute toxicity. Chronic Value (ChV) was used to demonstrate chronic toxicity.

3. Results and discussion

3.1. PMS-promoted degradation of HRAs

Advanced oxidation processes (AOPs) are considered as efficient techniques to degrade a wide range of contaminants owing to the generation of highly reactive radicals, e.g., $SO_4^{\bullet-}$ and $HO^{\bullet}$. Indeed, RNTD was susceptible to significant degradation in the UV/PDS and UV/HP

systems (Figure 2). In the UV/PMS system, RNTD degradation was much faster than that observed in UV/PDS or UV/HP systems, with complete degradation occurred after 2 min. Interestingly, PMS alone could also promote rapid degradation of RNTD; while the presence of PDS or HP alone exhibited negligible effect on RNTD degradation (Figure 2). PMS oxidation, reactive radical oxidation, and UV photodegradation could contribute to RNTD degradation in the UV/PMS system. The similar trend of RNTD degradation in PMS and UV/PMS system indicated that the contribution of PMS oxidation overwhelms other two degradation processes in UV/PMS system (Figure 2). Indeed, the decomposition of PMS was only slightly increased after introduction of UV irradiation (Figure S1). Hence, the rapid degradation of RNTD in UV/PMS system was most likely contributed from the PMS-promoted degradation. We further conducted radical quenching experiments to investigate whether radical species involved in the PMS-induced oxidation of RNTD. Generally, MeOH and TBA are always selected as the radical probes to distinguish $SO_4^{\bullet-}$ and $HO^{\bullet}$. MeOH reacts with $SO_4^{\bullet-}$ and $HO^{\bullet}$ at a comparable rate (9.7×10^8 $M^{-1}s^{-1}$, 3.2×10^6 $M^{-1}s^{-1}$ for $SO_4^{\bullet-}$ and $HO^{\bullet}$, respectively) ; while TBA reacts with $SO_4^{\bullet-}$ ($(4.0\text{-}9.1) \times 10^5$ $M^{-1}s^{-1}$) much slower than that with $HO^{\bullet}$ ($(3.8\text{-}7.6) \times 10^8$ $M^{-1}s^{-1}$) (Liang and Su 2009). As shown in Figure S2, the addition of alcohols did not affect the degradation of RNTD by PMS, even when the concentration of alcohols increased to 1000 mM. This result indicated that radical species did not involve in the PMS-promoted degradation of RNTD, and this reaction most likely proceeded via the non-radical process. It is noted that singlet oxygen ($^1O_2$) can be generated from the self-decomposition of PMS. Furfuryl alcohol (FFA, a scavenger for $^1O_2$ (Yang et al. 2018)) was added in PMS/RNTD solution, and the results showed that both RNTD degradation and PMS

decomposition were not affected after addition of FFA after 2 min (Figure S3), and thus $^1O_2$ did not contribute to the PMS-promoted degradation of RNTD. Hence, PMS likely exhibited specific reactivity towards RNTD.

We further investigated the degradation of other four HRAs by PMS to evaluate whether PMS shows specific reactivity towards all HRAs. As shown in Figure 3, PMS promoted rapid degradation of CMTD, FMTD and NZTD, but was inert for the degradation of RXTD. Hence, PMS-promoted degradation was dependent on HRAs' structure. HRAs possess several electron-rich moieties/groups, e.g., amine, which are always regarded as the potential reactive sites for oxidants. On the other hand, multiple amine moieties/groups are present in the investigated HRAs; while thioether sulfur occurs in CMTD, RNTD, FMTD and NZTD, but not in RXTD (Figure 1). It is thus suggested that the different reactivity of HRAs towards PMS likely related to the presence/absence of the thioether sulfur, which will be further elucidated in the following sections.

3.2 Degradation kinetics

The impact of HRAs concentration on the PMS-promoted degradation was investigated at neutral pH condition. As shown in Figure 4A, PMS-promoted HRAs degradation increased with PMS concentration increasing from 0.05 mM to 0.5 mM. Moreover, HRAs degradation followed pseudo-first-order kinetics at various PMS concentrations (equation 1), with the calculated pseudo-first-order constants (k_{obs}) demonstrated in Figure 4B. Log(k_{obs}) linearly increased with log(C_{PMS}), and the slope was close to unity. Hence, k_{obs} showed a linear relationship with respect to PMS concentration, suggesting the overall reaction could be

described by a second-order kinetics (equation 2). Apparent second-order reaction rate constants ($k_{2,app}$) could be obtained by dividing k_{obs} by PMS concentration. As shown in Figure 4C, $k_{2,app}$ was calculated to be 481.6 ± (16.7), 872 ± (57.9), 531.6 ± (36.2), 403 ± (21.5) $M^{-1}s^{-1}$ for RNTD, FMTD, CMTD and NZTD, respectively. The calculated $k_{2,app}$ values for HRAs were almost one order of magnitude higher than those for the reaction between PMS and β-lactam antibiotics (Chen et al. 2018) and tetracyclines (Chen et al. 2019a).

$$-\frac{d[HRAs]}{dt} = k_{obs-HRAs} \cdot [HRAs] \quad (1)$$

$$-\frac{d[HRAs]}{dt} = k_{2,app-HRAs} \cdot [HRAs] \cdot [PMS] \quad (2)$$

3.3 pH impact

The oxidation of organic contaminants by PMS was previously reported to depend on solution pH (Nihemaiti et al. 2020). Hence, pH impact was further examined for the degradation of HRAs by PMS at pH 3.0-9.0. As illustrated in Figure 5, PMS-promoted degradation of HRAs were pH-dependent. Generally, HRAs degradation by PMS was almost unaffected by the solution pH from 3.0 to 5.0. Afterwards, the values of $k_{2,app}$ slightly decreased with pH further increased to pH 7.0, and more sharply decreased when pH finally increased to pH 9.0. PMS possesses two pK_a values ($pK_{a1} < 0$, $pK_{a2} = 9.4$) (Zhang et al. 2013), and thus mainly exhibiting HSO_5^- and SO_5^{2-} species at the investigated pHs ($HSO_5^- \rightleftharpoons H^+ + SO_5^{2-}$, $pK_{a2} = 9.4$) (Figure S4). In addition, the pK_a values for the amine groups in HRAs were at around pH 7.0 (i.e., pKa = 8.2 (Latch et al. 2003), 7.1 (Latch et al. 2003), 6.7 (Echizen and Ishizaki 1991), and 6.8 (Wu et al. 2001) for RNTD, CMTD, FMTD and NZTD, respectively). Hence, HRAs exhibit the protonated state at the acidic pHs (pH 3.0 and 5.0),

but deprotonated state at pH 9.0 ($HRAs^0 \rightleftharpoons H^+ + HRAs^-$). The species-specific reaction between HRAs and PMS was used to explain the pH dependency of $k_{2,app}$ of HRAs (equation 3 and 4).

$$-\frac{d[HRAs]_T}{dt} = k_{2,app-HRAs} \cdot [HRAs]_T \cdot [PMS]_T$$

$$= \sum_{i,j}^{m,n} k_{i,j} \cdot \alpha_i \cdot \beta_j . [HRAs]_T \cdot [PMS]_T \quad (3)$$

Hence,

$$k_{2,app-HRAs} = \sum_{i,j}^{m,n} k_{i,j} \cdot \alpha_i \cdot \beta_j \quad (4)$$

where $[HRAs]_T$ and $[PMS]_T$ represent the total concentration of HRAs and PMS, respectively; $k_{i,j}$ represents the species-specific second-order rate constant for the reaction between species *i* of HRAs and species *j* of PMS; and α_i and β_j represent the distribution coefficients of HRAs and PMS species, respectively. The $k_{i,j}$ were obtained by least-squares regression of the experimental data of $k_{2,app-HRAs}$ to equation (4). Because of the small fraction of $HRAs^0$-SO_5^{2-} (Figure S5), and lower oxidation capacity of SO_5^{2-} than HSO_5^-, the specific reaction between $HRAs^0$ and SO_5^{2-} was not considered. As shown in Figure 5, the experimental data of $k_{2,app-HRAs}$ at various pHs could be well explained by the species-specific reactions. The values of $k_{i,j}$ are summarized in Table S4, and their contribution to the overall $k_{2,app}$ is described in Figure S6. Results show that the contribution of SO_5^{2-} could be neglected at pH 7 and below (Figure S6). Indeed, SO_5^{2-} showed relatively low reactivity towards HRAs (Table S4), and SO_5^{2-} were reported to possess lower oxidation capacity than HSO_5^- (Lei et al. 2016). Furthermore, $HRAs^0$ was more susceptible to oxidation with PMS than $HRAs^-$, which

is different from the fact that the deprotonated species with richer electrons normally react faster with oxidants. It was thus implied that the reaction site on HRAs towards PMS oxidation is not the deprotonated functional group, i.e., the amine groups on HRAs, which will be further discussed in the following sections. The higher reactivity of $HRAs^0$ towards PMS might be explained by electrostatic interactions. The negatively charged PMS could get close to the protonated HRAs more easily than the deprotonated HRAs, thus exhibited higher reactivity towards the protonated HRAs.

3.4 Impact of water matrices

We further evaluated the impact of water matrices on PMS-promoted degradation of HRAs with the results shown in Figure 6. Unlike the AOPs with radical generation, the addition of common anions, e.g., Cl^- (0-300 mM) and HCO_3^- (0-100 mM) did not affect the degradation of HRAs by PMS at neutral pH (Figure 6A and B), indicating these anions in water matrices exhibited negligible effect on PMS-promoted degradation of HRAs. Indeed, Cl^- reacts with HSO_5^- and SO_5^{2-} at the rate constants of 2.06×10^{-3} $M^{-1}s^{-1}$ and 3.8×10^{-4} $M^{-1}s^{-1}$, respectively (Lente et al., 2009), which are much lower than the rate constants between HRAs with PMS (403-872 $M^{-1}s^{-1}$). Hence, the impact of Cl^- on PMS-induced oxidation of HRAs could be negligible. Moreover, the degradation of HRAs was not affected in the presence of HA (0-50 mg/L) (Figure 6C), suggesting that the natural organic matter also showed neglectable effect on HRAs degradation. Organic matter and Cl^- are always known to affect $SO_4^{\bullet-}$, and thus the water matrices can compete with the target contaminants towards the radical consumption in AOPs, thus reducing the treatment efficiency (Chen et al. 2019b). The

negligible impact of water matrices on PMS-promoted HRAs degradation also implied that HRAs degradation was not primarily contributed from radicals.

We further investigated PMS-promoted degradation of HRAs in the real water samples. As shown in Figure 7, HRAs degradation in DI water was similar to those in the SW, HWW and MWW, thus the degradation of HRAs by PMS was not affected by the real water matrices. Moreover, we also evaluated the decomposition of PMS along the HRAs degradation in the real water matrices, and the results show that PMS decomposition was initially fast, and finally ceased (Figure S7). The trend of PMS decomposition resembled the degradation of HRAs, indicating that the decomposition of PMS was induced by the reaction with HRAs, but not by the water matrices. On the other hand, PMS decomposition was also not influenced by the real water matrices. These evidences further confirmed that PMS showed specific and rapid reactivity towards HRAs, which was not affected by the water matrices. Hence, compared to the AOPs with radical generation, PMS oxidation was a more appealing alternative for degradation of HRAs in real water matrices.

3.5. Reaction pathway and mechanism

3.5.1 Theoretical prediction of reaction sites

The abovementioned radical scavenging experiments verified the non-radical process for PMS-promoted HRAs degradation. The oxidation of HRAs most likely proceeded via electrophilic reaction by PMS. PMS tends to attack the moieties/groups with high electron density in HRAs. Indeed, the electron-rich moieties/groups in HRAs, such as double bonds, amine, sulfur were regarded as the potential sites susceptible to oxidation by various oxidants,

e.g., O_3, $KMnO_4$, Cl_2, and ClO_2 (Wang et al. 2016). Theoretical calculations were frequently used to predict the potential reaction sites in electrophilic reaction (Qu et al. 2015). Based on the frontier molecular orbital theory, the electrophilic reaction probably takes place at the electron rich (HOMO) regions, and the results were shown in Figure 8. Generally, the HOMO orbits cannot precisely describe the gain or loss of electron on each HRAs molecule site during reaction. Therefore, we also calculated the Fukui index on electrophilic attack (f^-) according to natural population analysis (NPA) charge distribution of HRAs molecule (Tables S5-S9). For the investigated HRAs (except RXTD), the HOMOs and f^- were mainly distributed on the double bond, sulfur, and nitrogen atoms, suggesting these sites might act as the potential reactive sites susceptible to PMS attack. For RXTD, however, the HOMOs primarily located on the double bond and the nitrogen atoms. Based on the abovementioned results that RXTD showed negligible reactivity towards PMS, sulfur atom (absence in RXTD) was likely the reactive sites for PMS oxidation. To facilitate discerning the reaction mechanism, the transformation products by PMS oxidation were further analyzed.

3.5.2 Transformation products

Transformation products of HRAs were further investigated by LC/MS/MS. The primary products with molecular weights (MW) of M+16 and M+32 (M: MW of the parent HRAs) were observed during PMS-promoted oxidation of HRAs (Figure 9). They were most probably the oxidation products with one/two oxygen addition on the parent HRAs, which were also observed in the direct oxidation of β-lactam antibiotics/tetracycline by PMS (Chen et al. 2018, Chen et al. 2019a). In the PMS-promoted oxidation, however, the product profile of HRAs was different from those of β-lactam antibiotics/tetracycline. For example, two or

more M+16 products were generated and verified as the isomers in PMS-promoted oxidation of β-lactam antibiotics (Chen et al. 2018); while the sole M+16 product was produced in HRAs degradation by PMS. On the other hand, M+16 products were generated via oxygen transfer from PMS to the thioether sulfur on the five (six)-membered ring of β-lactam antibiotics (Chen et al. 2018), but via hydroxylation process in the B ring of tetracycline (Chen et al. 2019a). It is still unclear how M+16 were generated in the PMS-promoted oxidation of HRAs. The structure of transformation products were thus analyzed based on the mass fragments.

RNTD

Both M+16 and M+32 products were generated in PMS-promoted oxidation of RNTD, and the intensity of M+16 was much higher than that of M+32 (Figure 9A). Hence, the reaction between PMS and RNTD primarily proceeded via the addition of one oxygen atom on RNTD. To evaluate the potential reactive sites on RNTD, we analyzed the bond cleavage of RNTD in the ESI fragmentation at first. In the mass spectrum of the parent compound RNTD (Figure S8), the presence of m/z 176/138, and m/z 170/144 indicated the breakage of the –S–C– bond, hence this site is susceptible to cleave in the reaction. Moreover, the m/z 130 is also observed in the spectrum of RNTD, especially at the higher fragmentation voltage, suggesting that the –C–C– near the sulfur atom is also likely to cleave during the reaction, but the required energy is higher than the cleavage of –S–C–. In addition, the fragment of m/z 270 was generated via the loss of N,N-dimethylamino moiety from RNTD, and further loss of $–NO_2$ of m/z 270 produced the fragment of m/z 224.

In the M+16 product, the presence of m/z 138 and m/z 110 fragments indicated the intact furan structure in RNTD (Figure S9). Hence, the oxygen addition site most likely located on the other side part of RNTD, which was verified by the presence of m/z 192 (192 = 176 +16, m/z 176 is the S containing structure in RNTD) in the M+16 product. Fragment of m/z 286 was generated from the loss of N,N-dimethylamine (45 Da) from RNTD, and further loss of H_2O (18 Da) generated the fragment ion m/z 268. It is noted that both RNTD and M+16 product contain fragment of m/z 130, suggesting the oxygen addition could not occur at the double bond on the right side (Figure S9). Hence, the –S–C– is the most likely site for oxygen addition. According to the theoretical calculation, HOMOs of sulfur atom is much higher than the neighboring carbon, thus sulfur is vulnerable to electrophilic attack by PMS. Indeed, the thioether sulfur was previously regarded as preferable site for PMS oxidation (Chen et al. 2018). Hence, M+16 product was supposed to be the sulfoxide product of RNTD.

Both the fragments of m/z 130 and m/z 138 were observed in the mass spectra of RNTD and its M+32 product (Figure S10), indicating the intact furan structure on the left side and the double bond on the right side in M+32 product. The –S–C– moiety is also the potential reactive sites for two oxygen atoms addition. In the RNTD sulfoxide, the oxygen is difficult to further add on the sulfur to generate sulfone products owing to the steric hindrance effect. The second oxygen is most likely to add on the carbon neighboring to sulfur and underwent via the hydroxylation process. This hypothesis was verified by the presence of m/z 192 fragment in the mass spectrum of M+32 product. Because of the extremely low intensity of M+32 product (Figure 9A), the hydroxylation at carbon neighboring sulfur on RNTD could be negligible compared to the oxidation at thioether sulfur on RNTD.

CMTD

Only M+16 product was observed in the reaction between PMS and CMTD (Figure 9 B). The prominent fragment of CMTD was m/z 159 (Figure S11), suggesting the –S–C– is liable to cleave, and thus this moiety is vulnerable to reactions. With the increasing fragmentation voltage, the intensity of m/z 117 increased along with the decreasing m/z 159 intensity, indicating the loss of –N–CN in CMTD. In M+16 product (Figure S12), the sulfur atom was most susceptible to electrophilic attack by PMS based on the theoretical calculation. Indeed, the presence of m/z 175 (175 = 159 + 16) and m/z 133 (133 = 117 + 16) also indicated that the oxygen atom likely added on the sulfur to generate CMTD sulfoxide product.

FMTD

The product profile of FMTD was similar to that of RNTD. Both M+16 and M+32 products were observed along FMTD oxidation (Figure 9C). The mass fragment pattern of FMTD resembled that of CMTD, that is, few fragments were observed even at high voltage (Figure S13). The presence of m/z 189 and m/z 155 indicated the cleavage of –S–C– moiety, while m/z 259 means the loss of $–SO_2–NH_2$ fragments. In M+16 product, the most abundant fragment is m/z 205 (Figure S14), indicating the oxygen addition likely occurred on the m/z 189 fragment in FMTD (205 = 189 + 16). Similarly, the presence of m/z 275 suggests the oxygen addition on m/z 259 in FMTD (275 = 259 + 16). On the other hand, the fragment of m/z 155 in M+16 product indicated the presence of intact thiazole ring. The fragments of m/z 275, 205 and 155 were also reported in the product of FMTD generated by the photo-catalytic oxidation, which was finally identified as sulfoxide of FMTD (Murphy et al. 2012). The

above evidences indicated that the oxygen addition was located on the sulfur atom, generating the FMTD sulfoxide product.

For M+32, the intensity of $[M+32+Na]^+$ is much higher than that of $[M+32+H]^+$, and the mass spectrum of $[M+32+Na]^+$ was obtained and shown in Figure S15. The presence of m/z 313 means the oxygen addition on m/z 259 fragment (313 = 259 + 32 – H + Na), and the loss of $–SO_2–NH_2$ fragments. Moreover, the appearance of m/z 243 indicated the second oxygen added on the left side of M+16 (243 = 205 + 16 – H + Na), probably on the sulfur on thiazole ring based on the theoretical calculation.

NZTD

Both M+16 and M+32 products were observed in PMS-promoted oxidation of NZTD (Figure 9D). In the mass spectrum of NZTD, the presence of m/z 155 and m/z 187 indicated the cleavage of –S–C– in the fragmentation (Figure S16). It is noted that NZTD and RNTD share the same right side in their structure (Figure 1), the cleavage of –S–C– in RNTD generated the primary fragment of m/z 176, which was not observed in NZTD. However, m/z 131 was observed in the fragments of NZTD, and its intensity increased as the most abundant fragment when the voltage increased to 30 eV. m/z 131 was supposed as the product of m/z 176 after loss of $–NO_2$. The appearance of m/z 286 also verified $–NO_2$ prone to lose in the fragmentation. According to the theoretical calculation, the sulfur atom and the C atom next to $–NO_2$ possess high HOMOs, consistent with the fragmentation patterns of NZTD.

In the M+16 product, the presence of m/z 130 and m/z 144 indicated the intact right side of NZTD (Figure S17), and thus the oxygen addition could not locate on the double bond next to

–NO_2. In addition, the appearance of fragments of m/z 205 and m/z 147 suggest the oxygen added on the sulfur on the straight chain. m/z 147 was supposed to be the addition of oxygen on m/z 131 fragment of NZTD, and the loss of –NO_2 in the right side. According to the evolution of transformation products, M+16 product initially increased and then gradually decreased. At the same time, the other product, i.e., M+32, continuously increased (Figure 9D). Hence M+16 product was further transformed to M+32 product, and the second oxygen likely added on M+16 product. The presence of m/z 147 and m/z 192 indicated an intact right side of M+16 (Figure S18), hence the second oxygen was likely added on the sulfur atom on thiazole ring based on the theoretical calculation.

Overall, M+16 and M+32 products were identified as the primary products of HRAs after reaction with PMS. Although the hydroxylation took place in the PMS-promoted degradation of RNTD to form M+32, its intensity was much lower than M+16, and thus this reaction process could be neglected in PMS promoted oxidation of HRAs. Oxidation of thioether sulfur to generate sulfoxide were supposed as the dominant mechanism for HRAs oxidation.

3.5.3 Reaction mechanism

The conventional PMS activation processes rely on the generation of radicals for contaminant destruction. In this work, PMS-promoted degradation of HRAs did not rely on radical generation, but proceeded via a direct oxidation. This mild process was previously reported to dominate in the oxidation of arsenite (Wang et al. 2014), hydrogen sulfide (Betterton and Hoffmann 1990), and β-lactam antibiotics by PMS (Chen et al. 2018). Generally, the direct oxidation process proceeds through two-electron transfer, which

involves the heterolytic breakage of the peroxide bond and an oxygen transfer from PMS to the contaminants (Figure 10). PMS was converted to sulfate ion upon reaction without $SO_4^{\bullet-}$ generation. Indeed, in the direct oxidation between PMS and HRAs, the symmetry-adapted configuration between 2p orbital of oxygen and empty 3d orbital in sulfur renders lone pair electrons of oxygen liable to donate to sulfur, generating a feedback coordination bond (Wang et al. 2016). This process results in an oxygen atom transfer from PMS to the thioether sulfur with the formation of HRAs sulfoxide. It is noted that two stereoisomeric sulfoxides were generated in β-lactam antibiotics oxidized by PMS (Chen et al. 2018). The fusion of β-lactam ring and five (or six)-membered ring makes the electrons of thioether sulfur on the ring more exposed outside, thus susceptible to peroxide attack from different directions. Such structure characteristic is not observed in HRAs, thus only one sulfoxide is generated in PMS-promoted oxidation of HRAs.

It is noted that multiple thioether sulfur containing moieties/groups are present in the structures of HRAs, e.g., FMTD and NZTD. Based on the transformation product analysis of FMTD and NZTD, both the thioether sulfurs on the straight chain and the thiazole ring show reactivity towards PMS oxidation. Moreover, the intensity of M+16 product was much higher than that of M+32 product, indicating that the thioether sulfur on the straight chain shows much higher reactivity towards PMS than that on the thiazole ring of HRAs. On the one hand, the Fukui index (f^-) of thioether sulfur on the straight chain was higher than that on the thiazole ring (Tables S6 and S7), hence the thioether sulfur on the straight chain was more susceptible to electrophilic attack by PMS than that on the thiazole ring. On the other hand, the amine groups adjacent to thioether sulfur on the thiazole ring might hinder the attack of

PMS on the thioether sulfur owing to the steric hindrance effect, thus contributing to the observed lower reactivity to PMS. These two factors induced the thioether sulfur on the straight chain in HRAs more susceptible to oxygen transfer with PMS.

Compared to the conventional PMS activation with radical generation, two electron transfer (i.e., oxygen atom transfer) process for HRAs oxidation exhibited high efficiency because the oxidation capacity of the peroxide were fully utilized. Moreover, the direct oxidation by PMS was not affected by the background ions and NOM in the water matrices, and thus showed high treatment efficiency in the real water matrices. Hence, this process could minimize the adverse impact of coexisting matrix constituent, and maximize the utilization efficiency of PMS. On the other hand, the oxidation of nitro-HRAs by conventional oxidants, e.g., ozone and chlorine, could generate the products with high TCNM formation potential (Wang et al. 2016); while the oxygen transfer process only involved the oxidation at thioether sulfur, but made little contribution to TCNM formation. Overall, direct oxidation by PMS is a facile and environmental-friendly strategy to alleviate HRAs contamination in the water.

3.6. Ecotoxicity evaluation

QSAR analysis was used to predict the ecotoxicity of contaminants and their products by ECOSAR program. As shown in Table 1, the acute toxicity was categorized as “not harmful” (> 100 mg/L) to fish for all the target contaminants, and classified as “harmful” (10-100 mg/L) to daphnid and green algae for CMTD and RNTD. Compared to the parent HRAs, the acute toxicity of the transformation products, e.g., M+16 and M+32 products belong to the “not harmful” category, and the LC50 (or EC50) values were ten times or even higher than

those of HRAs. Hence, acute toxicity of the HRAs could be significantly reduced after treatment with PMS.

For the chronic toxicity, CMTD and RNTD are classified as “toxic” (1-10 mg/L) compounds to daphnid, but “harmful” compounds to fish and algae; while their products have a significantly lower chronic toxicity with the ChV values on 1 order of magnitude higher than HRAs. Similarly, transformation products of FMTD and NZTD show much lower chronic toxicity than their corresponding parent contaminants. Overall, ecotoxicity of HRAs could be remarkably reduced after PMS treatment, and thus oxidation by PMS is a promising strategy to degrade HRAs and eliminate their toxicity.

4. Conclusions

PMS exhibits specific and high reactivity towards HRAs except RXTD, and the apparent second-order rate constants were determined to be in the range from 403 to 872 $M^{-1}s^{-1}$ at pH 7.0. Radical scavenging experiments confirmed lack of involvement of radical species. This non-radical process was not influenced by the water matrices, and thus maintained high efficiency in wastewater treatment. Theoretical calculations and transformation product analysis indicated that the thioether sulfur in HRAs (except RNTD) was the site susceptible to PMS oxidation, and was oxidized to the corresponding sulfoxide product. Toxicity evaluation indicated the ecotoxicity of HRAs was remarkably decreased after PMS oxidation. This work highlights a promising and facile strategy for alleviating HRA contamination in water treatment.

Acknowledgements

We sincerely thank the National Natural Science Foundation of China (51708097, 51878431), State Key Laboratory of Pollution Control and Resource Reuse Foundation (NO. PCRRF18007), and Fundamental Research Funds for the Central Universities (NO. 2232018D3-08).

References

Andreozzi, R., Raffaele, M., Nicklas, P., 2003. Pharmaceuticals in STP effluents and their solar photodegradation in aquatic environment. Chemosphere 50 (10), 1319-1330.

Anipsitakis, G.P., Dionysiou, D.D., 2004. Radical Generation by the Interaction of Transition Metals with Common Oxidants. Environ. Sci. Technol. 38 (13), 3705-3712.

Besse, J.-P., Garric, J., 2008. Human pharmaceuticals in surface waters: Implementation of a prioritization methodology and application to the French situation. Toxicol. Lett. 176 (2), 104-123.

Betterton, E.A., Hoffmann, M.R., 1990. Kinetics and mechanism of the oxidation of aqueous hydrogen sulfide by peroxymonosulfate. Environ. Sci. Technol. 24 (12), 1819-1824.

Buth, J.M., Arnold, W.A., McNeill, K., 2007. Unexpected products and reaction mechanisms of the aqueous chlorination of cimetidine. Environ. Sci. Technol. 41 (17), 6228-6233.

Chen, J., Fang, C., Xia, W., Huang, T., Huang, C.-H., 2018. Selective Transformation of β-Lactam Antibiotics by Peroxymonosulfate: Reaction Kinetics and Nonradical Mechanism. Environ. Sci. Technol. 52(3), 1461-1470.

Chen, J., Qian, Y., Liu, H., Huang, T., 2016a. Oxidative degradation of diclofenac by thermally activated persulfate: implication for ISCO. Environ. Sci. Pollut. R. 23(4), 3824-3833.

Chen, J., Xu, J., Liu, T., Qian, Y., Zhou, X., Xiao, S., Zhang, Y., 2019a. Selective oxidation of tetracyclines by peroxymonosulfate in livestock wastewater: Kinetics and non-radical mechanism. J. Hazard. Mater. 121656.

Chen, J., Zhang, L., Huang, T., Li, W., Wang, Y., Wang, Z., 2016b. Decolorization of azo dye by peroxymonosulfate activated by carbon nanotube: Radical versus non-radical mechanism. J. Hazard. Mater. 320, 571-580.

Chen, J., Zhou, X., Sun, P., Zhang, Y., Huang, C.-H., 2019b. Complexation Enhances Cu(II)-Activated Peroxydisulfate: A Novel Activation Mechanism and Cu(III) Contribution. Environ. Sci. Technol. 53(20), 11774-11782.

Choi, K., Kim, Y., Park, J., Park, C.K., Kim, M., Kim, H.S., Kim, P., 2008. Seasonal variations of several pharmaceutical residues in surface water and sewage treatment plants of Han River, Korea. Sci. Total Environ. 405(1-3), 120-128.

Dong, H., Qiang, Z., Lian, J., Qu, J., 2017. Degradation of nitro-based pharmaceuticals by UV photolysis: Kinetics and simultaneous reduction on halonitromethanes formation potential. Water Res. 119, 83-90.

Duan, X., Sun, H., Shao, Z., Wang, S., 2018. Nonradical reactions in environmental remediation processes: Uncertainty and challenges. Appl. Catal. B-Environ. 224, 973-982.

Echizen, H., Ishizaki, T., 1991. Clinical Pharmacokinetics of Famotidine. Clin.

Pharmacokinet. 21(3), 178-194.

Furman, O.S., Teel, A.L., Watts, R.J., 2010. Mechanism of Base Activation of Persulfate. Environ. Sci. Technol. 44(16), 6423-6428.

Ganellin, C.R., Durant, G.J., Emmett, J.C., 1976. Some chemical aspects of histamine H2-receptor antagonists. Fed. Proc. 35(8), 1924-1930.

Gao, H., Chen, J., Zhang, Y., Zhou, X., 2016. Sulfate radicals induced degradation of Triclosan in thermally activated persulfate system. Chem. Eng. J. 306, 522-530.

Ikehata, K., Jodeiri Naghashkar, N., Gamal El-Din, M., 2006a. Degradation of aqueous pharmaceuticals by ozonation and advanced oxidation processes: a review. Ozone-Sci. Eng. 28(6), 353-414.

Ikehata, K., Jodeiri Naghashkar, N., Gamal El-Din, M., 2006b. Degradation of Aqueous Pharmaceuticals by Ozonation and Advanced Oxidation Processes: A Review. Ozone-Sci. Eng. 28(6), 353-414.

Ji, Y., Lu, J., Wang, L., Jiang, M., Yang, Y., Yang, P., Zhou, L., Ferronato, C., Chovelon, J.-M., 2018. Non-activated peroxymonosulfate oxidation of sulfonamide antibiotics in water: Kinetics, mechanisms, and implications for water treatment. Water Res. 147, 82-90.

Kolpin, D.W., Furlong, E.T., Meyer, M.T., Thurman, E.M., Zaugg, S.D., Barber, L.B., Buxton, H.T., 2002. Pharmaceuticals, hormones, and other organic wastewater contaminants in US streams, 1999− 2000: A national reconnaissance. Environ. Sci. Technol. 36(6), 1202-1211.

Latch, D.E., Stender, B.L., Packer, J.L., Arnold, W.A., McNeill, K., 2003. Photochemical Fate of Pharmaceuticals in the Environment: Cimetidine and Ranitidine. Environ. Sci.

Technol. 37(15), 3342-3350.

Lente, G., Kalmár, J., Baranyai, Z., Kun, A., Kék, I., Bajusz, D., Takács, M., Veres, L., Fábián, I., 2009. One- versus two-electron oxidation with peroxomonosulfate ion: reactions with iron(II), vanadium(IV), halide ions, and photoreaction with cerium(III). Inorg. Chem. 48 (4), 1763-1773.

Lei, Y., Chen, C.-S., Ai, J., Lin, H., Huang, Y.-H., Zhang, H., 2016. Selective decolorization of cationic dyes by peroxymonosulfate: non-radical mechanism and effect of chloride. RSC Adv. 6(2), 866-871.

Liang, C., Huang, C.-F., Mohanty, N., Kurakalva, R.M., 2008. A rapid spectrophotometric determination of persulfate anion in ISCO. Chemosphere 73(9), 1540-1543.

Liang, C. and Su, H.-W., 2009. Identification of Sulfate and Hydroxyl Radicals in Thermally Activated Persulfate. Ind. Eng. Chem. Res. 48(11), 5558-5562.

Liu, T., Yin, K., Liu, C., Luo, J., Crittenden, J., Zhang, W., Luo, S., He, Q., Deng, Y., Liu, H., Zhang, D., 2018. The role of reactive oxygen species and carbonate radical in oxcarbazepine degradation via UV, UV/H2O2: Kinetics, mechanisms and toxicity evaluation. Water Res. 147, 204-213.

Murphy, S., Saurel, C., Morrissey, A., Tobin, J., Oelgemöller, M., Nolan, K., 2012. Photocatalytic activity of a porphyrin/TiO2 composite in the degradation of pharmaceuticals. Appl. Catal. B-Environ. 119-120, 156-165.

Nihemaiti, M., Permala, R.R., Croué, J.-P., 2020. Reactivity of unactivated peroxymonosulfate with nitrogenous compounds. Water Res. 169, 115221.

Pan, X., Chen, J., Wu, N., Qi, Y., Xu, X., Ge, J., Wang, X., Li, C., Qu, R., Sharma, V.K.,

Wang, Z., 2018. Degradation of aqueous 2,4,4′-Trihydroxybenzophenone by persulfate activated with nitrogen doped carbonaceous materials and the formation of dimer products. Water Res. 143, 176-187.

Qian, Y., Guo, X., Zhang, Y., Peng, Y., Sun, P., Huang, C.-H., Niu, J., Zhou, X., Crittenden, J.C., 2016. Perfluorooctanoic Acid Degradation Using UV-Persulfate Process: Modeling of the Degradation and Chlorate Formation. Environ. Sci. Technol. 50(2), 772-781.

Qian, Y., Xue, G., Chen, J., Luo, J., Zhou, X., Gao, P., Wang, Q., 2018. Oxidation of cefalexin by thermally activated persulfate: Kinetics, products, and antibacterial activity change. J. Hazard. Mater. 354, 153-160.

Qu, R., Xu, B., Meng, L., Wang, L., Wang, Z., 2015. Ozonation of indigo enhanced by carboxylated carbon nanotubes: Performance optimization, degradation products, reaction mechanism and toxicity evaluation. Water Res. 68, 316-327.

Radjenović, J., Petrović, M., Barceló, D., 2009. Fate and distribution of pharmaceuticals in wastewater and sewage sludge of the conventional activated sludge (CAS) and advanced membrane bioreactor (MBR) treatment. Water Res. 43(3), 831-841.

Serna-Galvis, E.A., Ferraro, F., Silva-Agredo, J., Torres-Palma, R.A., 2017. Degradation of highly consumed fluoroquinolones, penicillins and cephalosporins in distilled water and simulated hospital wastewater by UV254 and UV254/persulfate processes. Water Res. 122(Supplement C), 128-138.

Wang, X., Zhou, B., Yang, H., Wang, X., Xie, Y., 2016. Effect of oxidation on nitro-based pharmaceutical degradation and trichloronitromethane formation. Chemosphere 146, 154-161.

Wang, Z., Bush, R.T., Sullivan, L.A., Chen, C., Liu, J., 2014. Selective Oxidation of Arsenite by Peroxymonosulfate with High Utilization Efficiency of Oxidant. Environ. Sci. Technol. 48(7), 3978-3985.

Wu, S.-M., Ho, Y.-H., Wu, H.-L., Chen, S.-H., Ko, H.-S., 2001. Simultaneous determination of cimetidine, famotidine, nizatidine, and ranitidine in tablets by capillary zone electrophoresis. ELECTROPHORESIS 22(13), 2758-2762.

Yang, Y., Banerjee, G., Brudvig, G.W., Kim, J.-H., Pignatello, J.J., 2018. Oxidation of Organic Compounds in Water by Unactivated Peroxymonosulfate. Environ. Sci. Technol. 52(10), 5911-5919.

Yin, R., Guo, W., Wang, H., Du, J., Zhou, X., Wu, Q., Zheng, H., Chang, J., Ren, N. (2018) Selective degradation of sulfonamide antibiotics by peroxymonosulfate alone: Direct oxidation and nonradical mechanisms. Che. Eng. J. 334, 2539-2546.

Zhang, B.T., Zhang, Y., Teng, Y.H., Fan, M.H., 2015a. Sulfate Radical and Its Application in Decontamination Technologies. Crit. Rev. Env. Sci. Tec. 45(16), 1756-1800.

Zhang, Q., Chen, J., Dai, C., Zhang, Y., Zhou, X., 2015b. Degradation of carbamazepine and toxicity evaluation using the UV/persulfate process in aqueous solution. J. Chem. Technol. Bio. 90(4), 701-708.

Zhang,T., Zhu,H., Croué, J.-P., 2013.Production of Sulfate Radical from Peroxymonosulfate Induced by a Magnetically Separable CuFe2O4 Spinel in Water: Efficiency, Stability, and Mechanism. Environ. Sci. Technol. 47(6), 2784-2791.

Zhou, X., Liu, D., Zhang, Y., Chen, J., Chu, H., Qian, Y., 2018a. Degradation mechanism and kinetic modeling for UV/peroxydisulfate treatment of penicillin antibiotics. Chem Eng.

J. 341, 93-101.

Zhou, Y., Gao, Y., Pang, S.-Y., Jiang, J., Yang, Y., Ma, J., Yang, Y., Duan, J., Guo, Q., 2018b. Oxidation of fluoroquinolone antibiotics by peroxymonosulfate without activation: Kinetics, products, and antibacterial deactivation. Water Res. 145, 210-219.

Zuccato, E., Calamari, D., Natangelo, M. Fanelli, R., 2000. Presence of therapeutic drugs in the environment. The lancet 355(9217), 1789-1790.

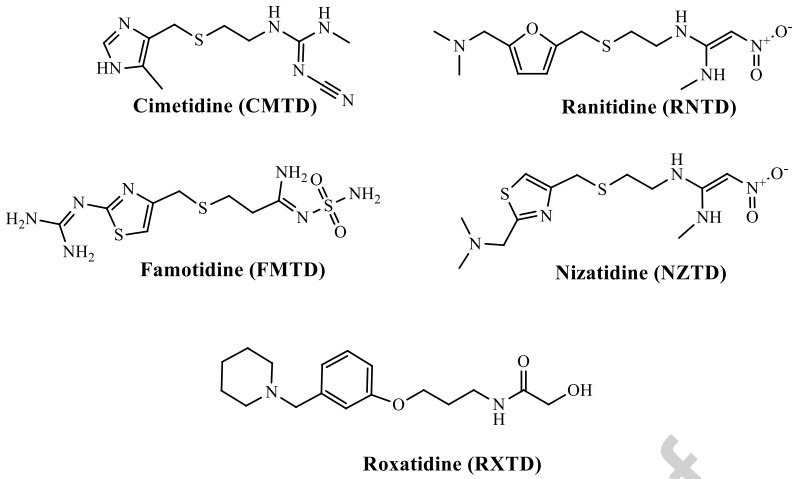

Figure 1. Chemical structures

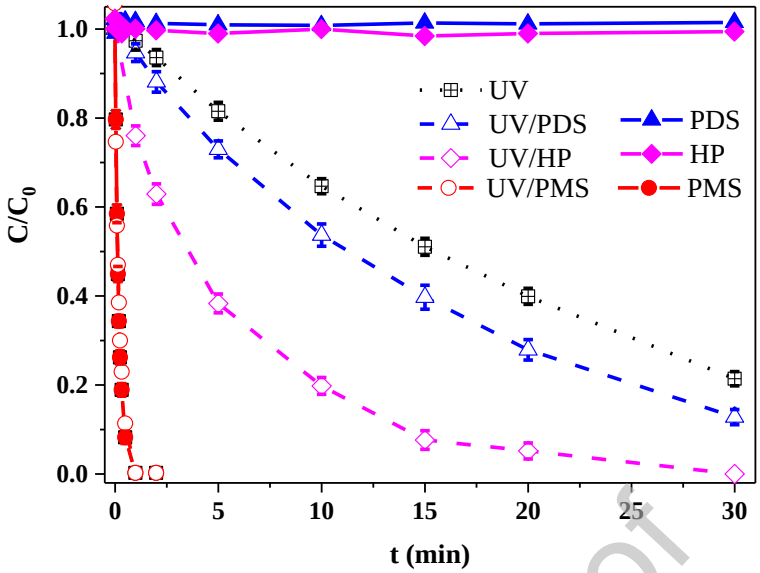

Figure 2. Degradation of RNTD by various peroxides and UV/peroxides. [RNTD] = 10 μM, [peroxide] = 100 μM, and pH 7.0.

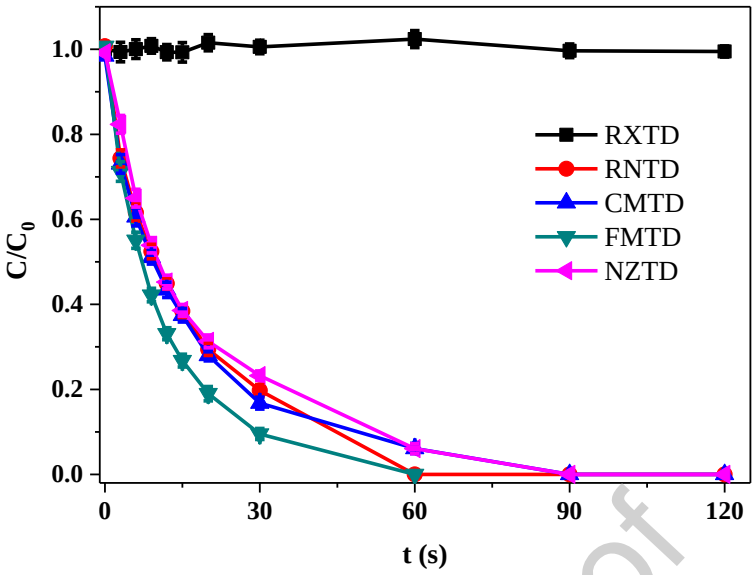

Figure 3. Degradation of various HRAs by PMS. Conditions: [HRAs] = 10 μM, [PMS] = 100 μM, pH 7.0.

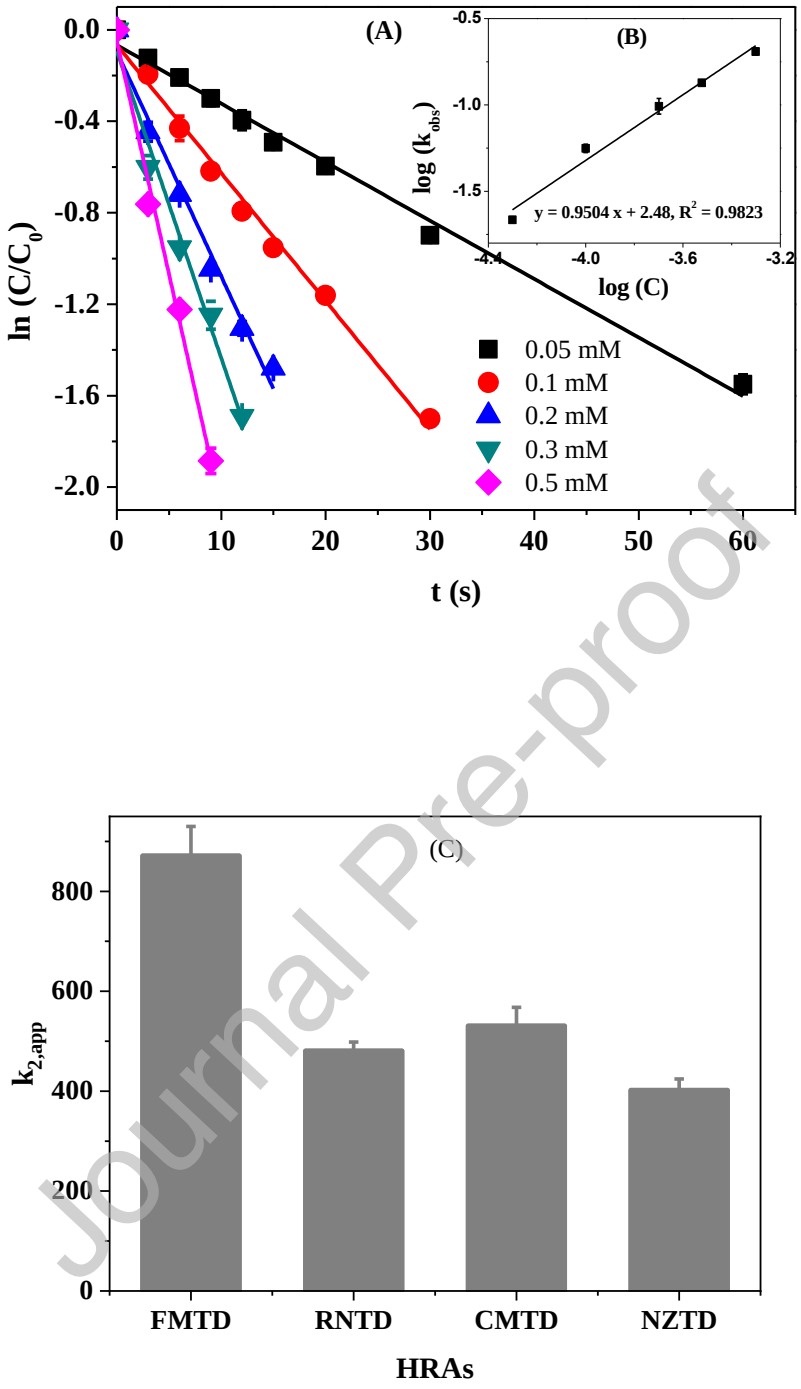

Figure 4. Effect of PMS concentration on RNTD degradation (A), and log ($k_{obs\text{-}RNTD}$) vs log (C_{PMS}) (B), and the second-order rate constants for various HRAs (C). [HRAs] = 10 μM, pH 7.0.

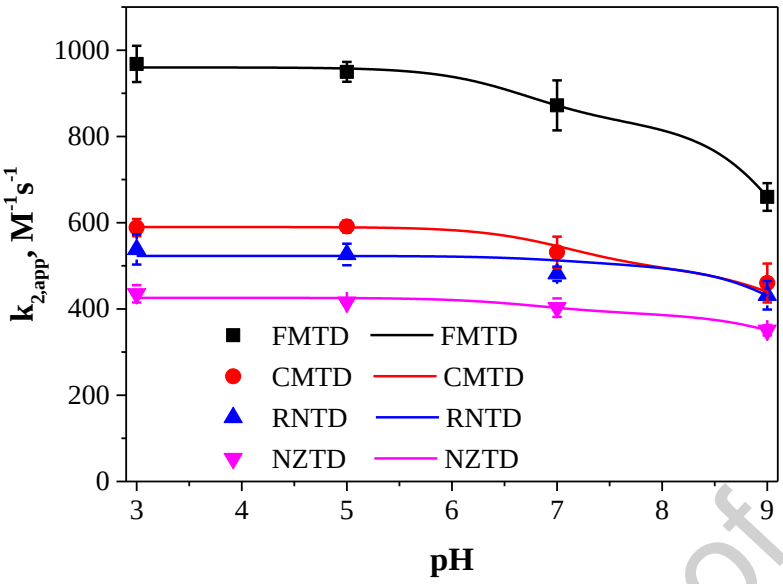

Figure 5. Impact of pH and kinetic modeling for the reaction rate constants of HRAs with PMS. Symbol: experimental $k_{2,app}$, Line: modeled $k_{2,app}$.

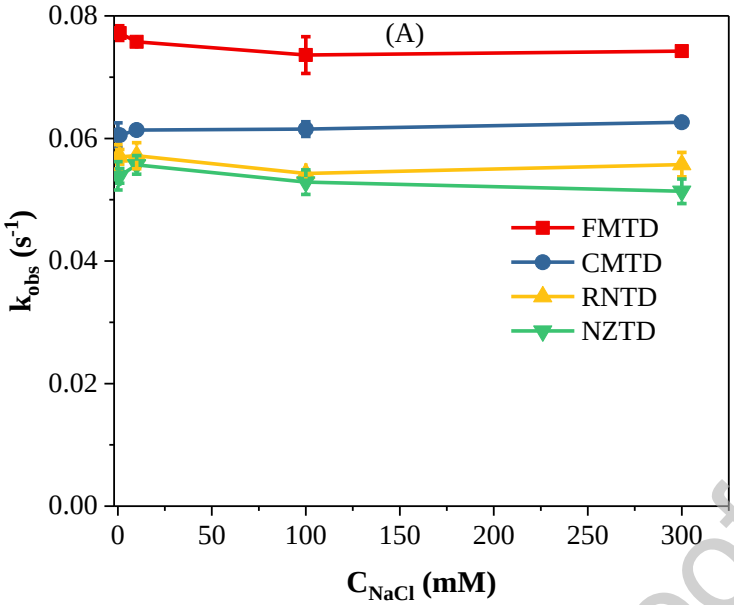

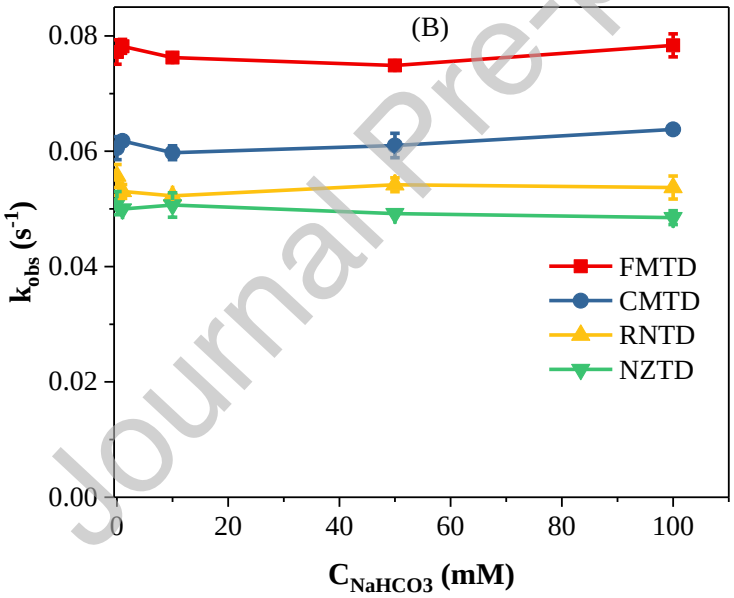

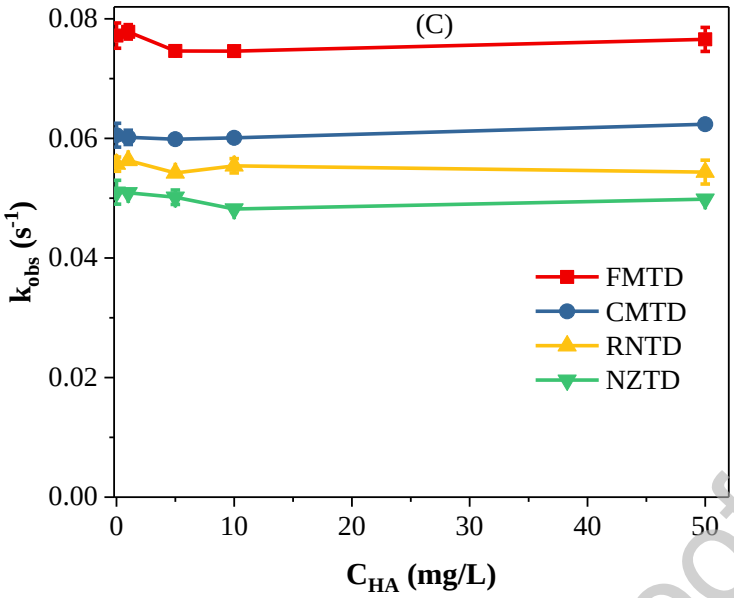

Figure 6. Impact of Cl^- (A), HCO_3^- (B), and HA (C) on k_{obs} of HRAs. [HRAs] = 10 μM, PMS = 100 μM and pH 7.0.

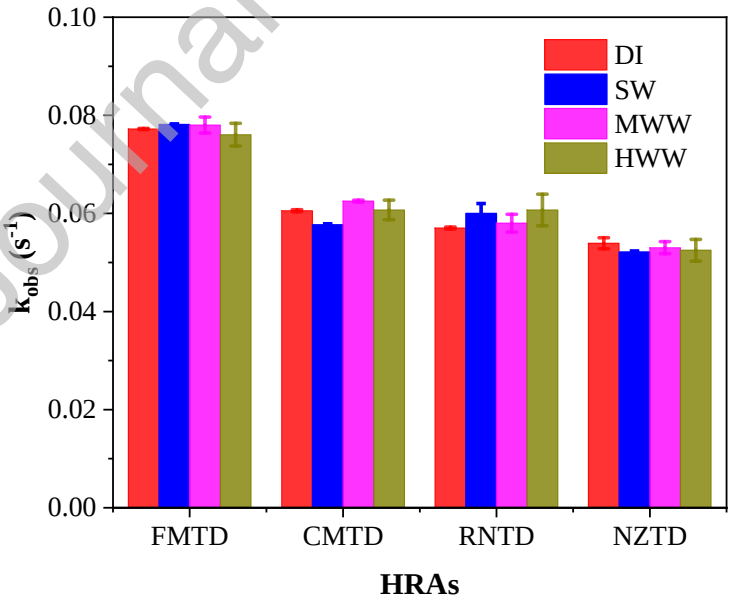

Figure 7. PMS-promoted degradation of HRAs in real water matrices. [HRAs] = 10 μM, PMS = 100 μM and pH 7.0.

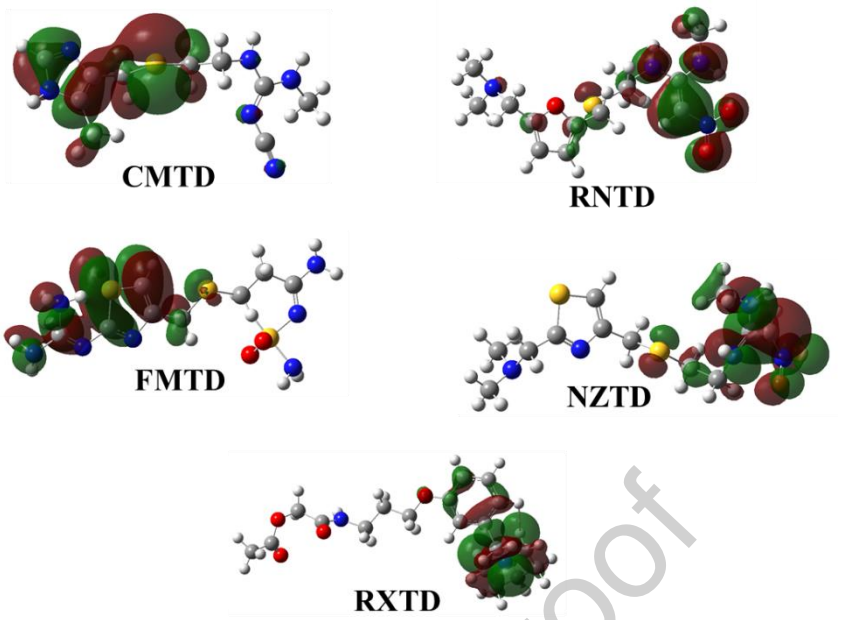

Figure 8. HOMOs of various HRAs. Note: The red and green colors represent the positive and negative phases of the molecular orbital of HRAs, respectively.

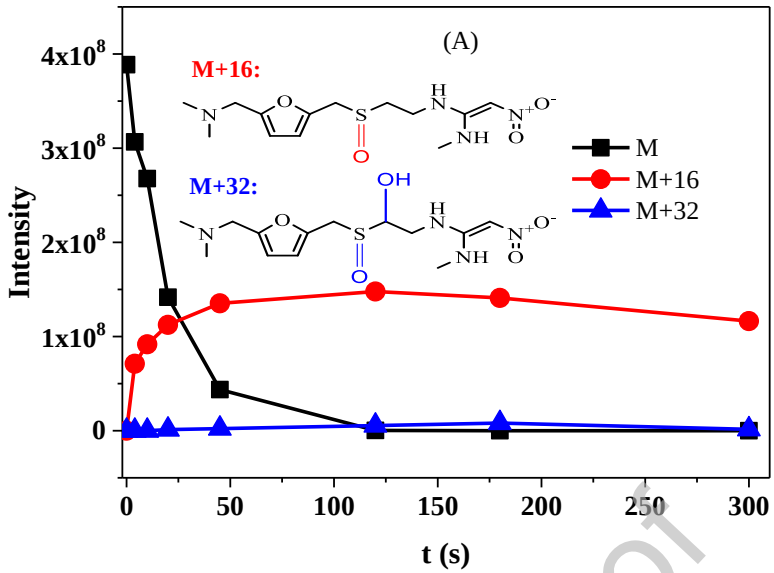

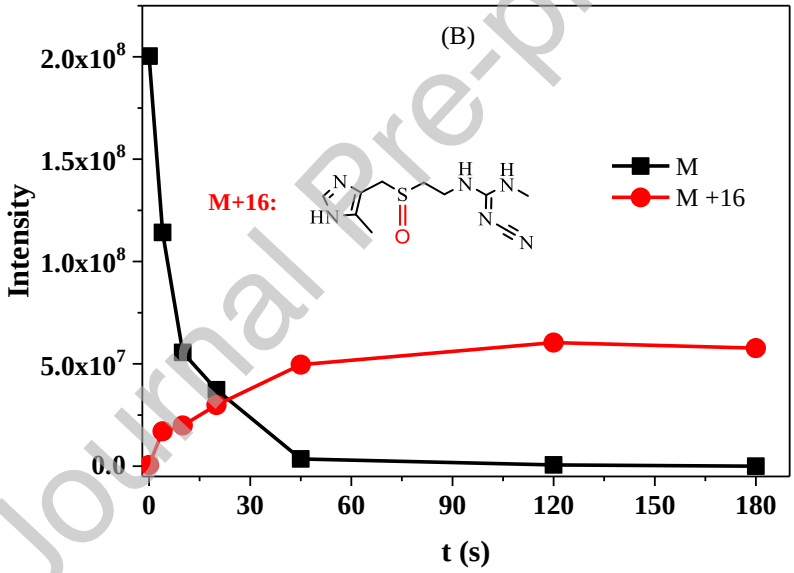

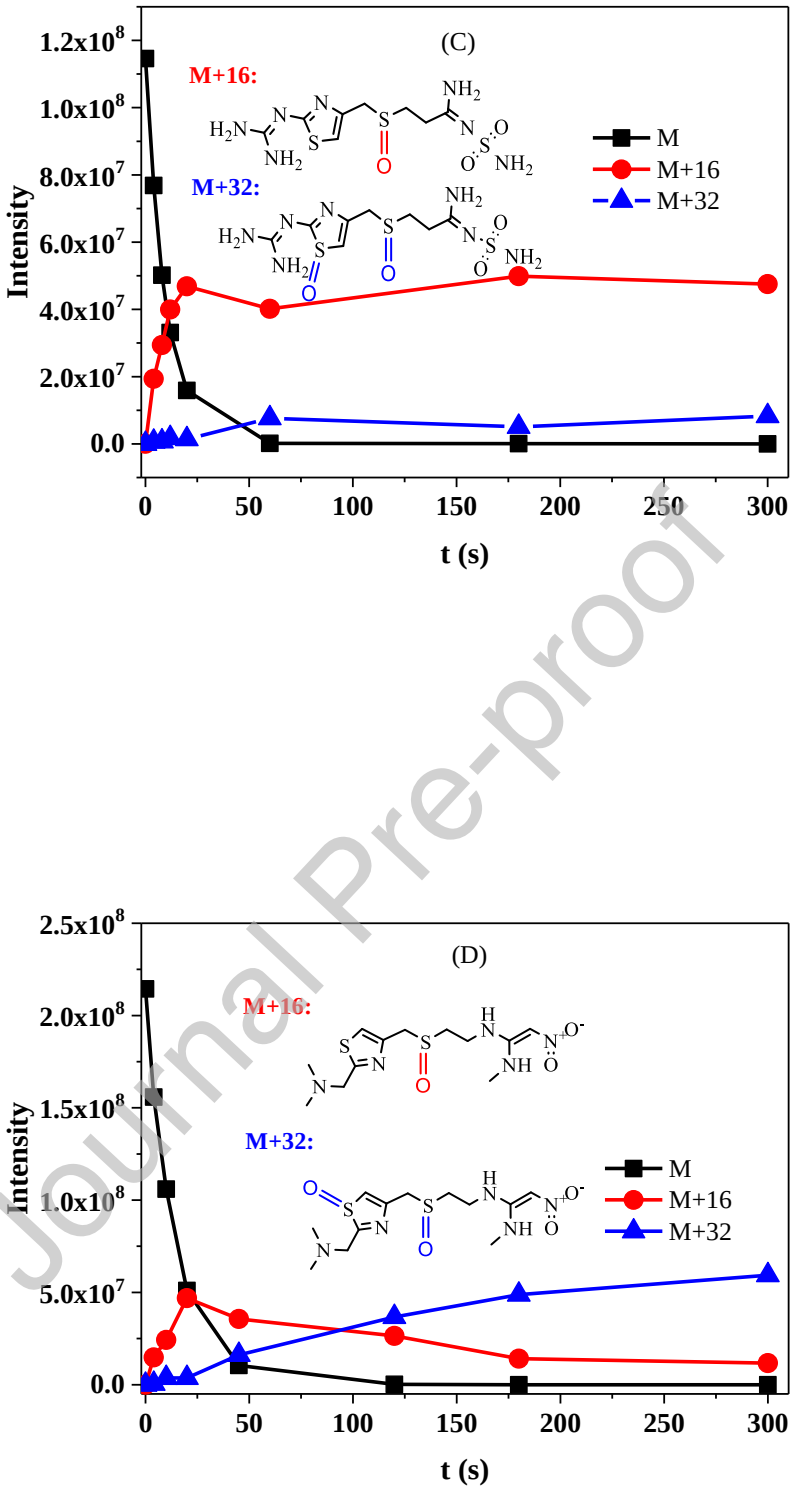

Figure 9. Transformation products of RNTD (A), CMTD (B), FMTD (C) and NZTD (D).

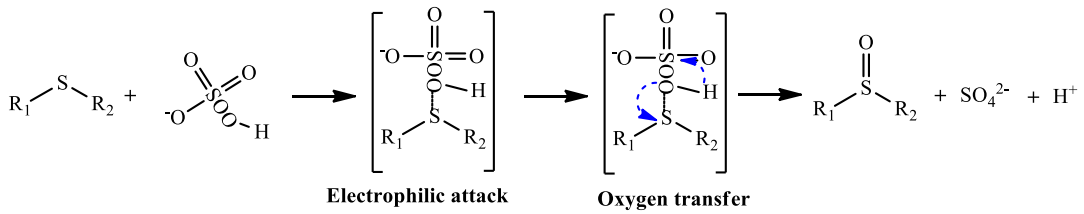

Figure 10. Proposed mechanism of PMS-promoted oxidation of HRAs. Note: R_1 and R_2 are side chains of thioether sulfur in HRAs.

Table 1. Estimated acute and chronic toxicity for fish, daphnid and green algae of HRAs and their products by ECOSAR.

Compound	Acute toxicity [a]			Chronic toxicity [a]		
	Fish (LC_{50} [b])	Daphnid (LC_{50} [b])	Green algae (EC_{50} [c])	Fish (ChV [d])	Daphnid (ChV [d])	Green algae (ChV [d])
CMTD	419	42.3	48.5	40.5	2.96	14.3
CMTD+16	1.14E+4	896	1.68E+3	2.34E+3	49.2	413
FMTD	3.59E+3	315	478	536	19.1	127
FMTD+16	9.61E+4	6.56E+3	1.63E+4	3.06E+4	313	3.62E+3
FMTD+32	2.95E+7	1.30E+6	7.66E+6	3.55E+7	4.06E+4	1.24E+6
NZTD	2.52E+3	227	327	348	14.1	88.6
NZTD+16	7.65E+4	4.73E+3	1.12E+4	1.99E+4	231	2.53E+3
NZTD+32	1.88E+5	1.22E+4	3.36E+4	6.98E+4	557	7.19E+3
RNTD	798	78.0	95.3	85.0	5.28	27.4
RNTD+16	2.14E+4	1.63E+3	3.26E+3	4.87E+3	86.7	784
RNTD+32	2.48E+5	1.57E+4	4.52E+4	9.91E+4	697	9.51E+3

[a] mg/L.

[b] LC_{50}: Median Lethal Concentration. A statistically derived concentration of a substance that can be expected to cause death in 50% of test animals.

[c] EC_{50}: Median Effect Concentration. A statistically derived concentration of a substance that can be expected to cause a specific effect (e.g., growth inhibition) in 50% of test animals.

[d] ChV is defined as the geometric mean of the no observed effect concentration and the lowest observed effect concentration.

Declaration of interests

☒ The authors declare that they have no known competing financial interests or personal relationships that could have appeared to influence the work reported in this paper.

☐The authors declare the following financial interests/personal relationships which may be considered as potential competing interests:

Graphical abstract